ADVANCED OPTICAL MATERIALS
www.advopticalmat.de

Cucurbit[8]uril Induced Molecular Folding Cascade Assembly for NIR Targeted Cell Imaging

*Xiaolu Zhou, Xue Bai, Xuejian Zhang, Jing Wu, and Yu Liu**

A macrocyclic confinement-activated green phosphorescence and two-photon near-infrared (NIR) fluorescence supramolecular cascade assembly is constructed by multivalent interaction based on the alkyl-bridged triphenylamine-vinyl pyridine salts (BTPA), cucurbit[8]uril (CB[8]), β-cyclodextrin-grafted hyaluronic acid (HACD), and 4-bromophenyl pyridine salt and CB[8] complex (PY/CB[8]). Taking advantage of CB[8]-induced macrocyclic confinement and molecular folding, the fluorescence of BTPA is effectively redshifted by 30 nm from 720 to 750 nm. Subsequently, HACD, a cancer cell targeting agent, is co-assembled with a BTPA/CB[8] supramolecular folder to form a nanoparticle, further enhancing NIR fluorescence from 750 nm up to 810 nm through cascade confinement. Upon introduction of the 2:1 complex PY/CB[8], multicomponent nanoparticles are fabricated, not only showing efficient NIR fluorescence with an increase in quantum yield from 7.21% to 22.92% but also endowing green phosphorescence emission, which is successfully applied for two-photon cancer cell-targeted imaging to shield background interference from fluorescent and phosphorescent resources.

1. Introduction

Given the advantages of low photodamage, deep tissue penetration, and high signal-to-noise ratio, pure organic near-infrared (NIR) luminescence (> 650 nm) materials in aqueous solutions have become an attractive option in biological imaging.[1] In particular, the NIR materials with two-photon absorption[2] have received rising attention in recent years, which address the imaging depth constraints of conventional two-photon fluorescence modality with NIR excitation and visible light emission, owing to the suboptimal emission wavelength. Currently, the most prevalent strategies employed to extend the emission/excitation wavelengths into the NIR region involve strengthening the degree of π-conjugation via multiple aromatic blocks[3] and modifying the appropriate donor–acceptor (D–A) units.[1c,4] However, these approaches often require complex synthesis and suffer from poor water solubility, hindering their further practical applications. Therefore, significant effort was devoted to developing a platform that combines excellent luminescence properties with exceptional biocompatibility. Among them, the supramolecular macrocyclic self-assembly has emerged as a promising approach not only to construct multiple luminescent materials,[5] including NIR emission and room-temperature phosphorescence (RTP), but also shown to be avirulent with good internalization in cancer cell lines, which significantly improve the biocompatibility of organic molecule broadening the application scope in biological systems.[6] For instance, George and co-workers reported an aqueous RTP system with high quantum yields by utilizing a cucurbit[7]uril–phthalimide derivative complex based on host-guest interactions.[7] Tian and co-workers constructed a 2:2 complex composed of a 4-(4-bromophenyl)pyridine derivative and CB[8], which achieved efficient RTP emission through a CB[8]-stabilized intermolecular charge transfer (CT) state.[8] Huang and co-workers developed a NIR supramolecular nanoparticle through host-guest interactions between pillar[5]arene (WP5) and cyano stilbene derivatives and applied it in living cell imaging.[9] Our group also reported a multivalent supramolecular assembly consisting of anthracene-vinyl pyridine derivatives, cucurbit[8]uril(CB[8]) and amphiphilic calixarene, which displayed two-stage NIR fluorescence enhancement that allowed for lysosome-targeted cell imaging.[10] Furthermore, several commercially available dyes can be incorporated into multivalent supramolecular macrocyclic assemblies to establish a phosphorescence energy transfer platform, delivering a prolonged NIR emission.[11] Although numerous attempts have been undertaken to develop multivalent self-assembled luminescent systems, cascaded enhanced dual emission systems composed of two-photon NIR fluorescence and phosphorescent concurrently featuring targeted cancer cell imaging capacity have not been reported to the best of our knowledge.

Herein, we report a supramolecular macrocyclic cascade confinement-activated NIR fluorescence and green phosphorescence assembly consisting of alkyl-bridged triphenylamine-vinyl

X. Zhou, X. Bai, X. Zhang, Y. Liu
College of Chemistry
State Key Laboratory of Elemento Organic Chemistry
Nankai University
Tianjin 300071, P. R. China
E-mail: yuliu@nankai.edu.cn
J. Wu
China Medical and Health Analysis Center
Peking University
Beijing 100191, P. R. China

The ORCID identification number(s) for the author(s) of this article can be found under https://doi.org/10.1002/adom.202301550

DOI: 10.1002/adom.202301550

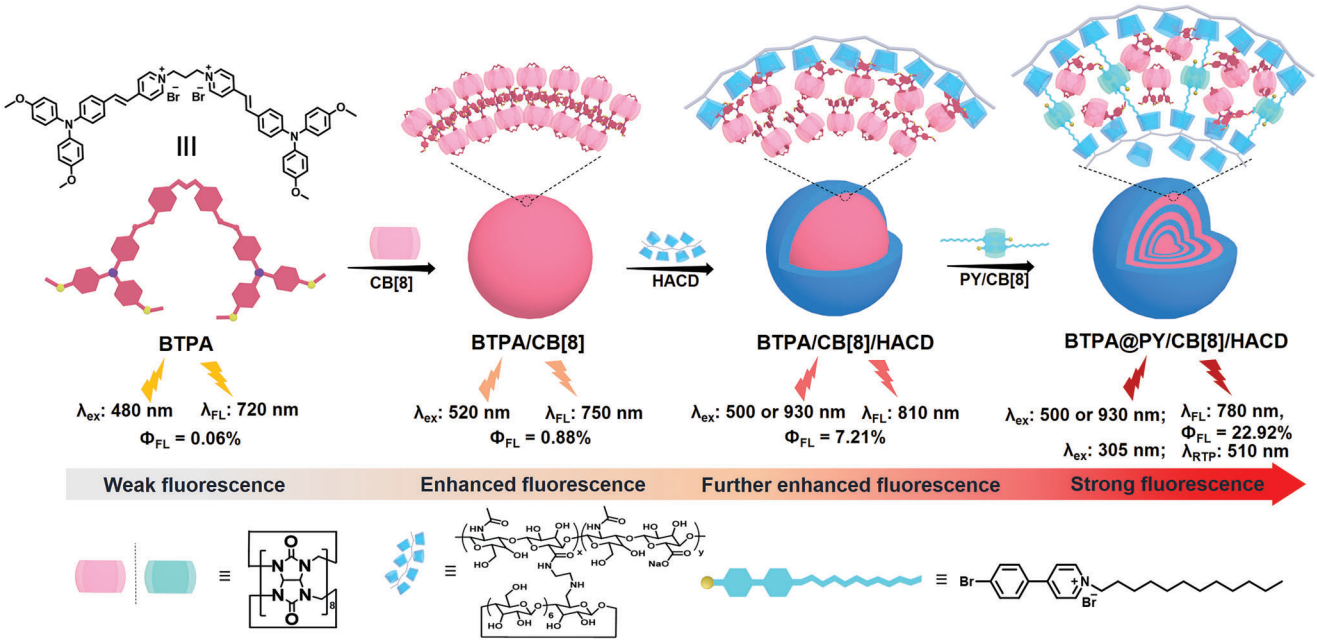

Scheme 1. Schematic illustration of cascade self-assembly for enhanced fluorescence behavior based on multivalent interaction.

pyridine salts (BTPA) with D-π-A structure, 4-bromophenyl pyridine salt derivative (PY), cucurbit[8]uril (CB[8]) and β-cyclodextrin-grafted hyaluronic acid (HACD), which exhibit cascade luminescent enhancement effect with a significant increase in quantum yield more than 380 times, and achieve targeted cancer cell imaging (**Scheme 1**). Specifically, the first macrocyclic confinement of CB[8] drives the guest molecule BTPA folding to form an intramolecular dimer, promoting a redshift in fluorescence from 720 to 750 nm and enhancing the luminescence quantum yield from 0.06% to 0.88% by restraining the stability of singlet excitons. The secondary assembly with HACD further facilitates the fluorescent quantum yield up to 7.21% and redshifts the emission from 750 to 810 nm, owing to the multivalent interaction between HACD and BTPA/CB[8]. Finally, via the introduction of PY/CB[8], a multicomponent supramolecular nanoparticle is constructed, which presents a green phosphorescent emission and a stronger NIR fluorescence with a high quantum yield of 22.92%. Remarkably, due to the intramolecular charge transfer (ICT) and overexpressed HA receptors of cancer cells, the homogeneous nanoparticles generated through multivalent supramolecular macrocyclic confinement exhibit two-photon absorption and realize targeted imaging of cancer cells. This intriguing property highlights the potential of this macrocyclic supramolecular cascade enhancement effect as a convenient strategy for obtaining efficient luminescent materials in the biomedical field and enabling the realization of fluorescent-phosphorescent targeted imaging techniques.

2. Results and Discussion

It is well known that CB[8] could bind with positively charged guests to form a stable complex with stoichiometric ratios of 1:1 or 1:2 through cation–dipole and hydrophobic interactions, and possess enhanced luminescence effects accompanied by redshift emission spans the UV–visible to the NIR region.[12] In order to investigate the luminescence effect of macrocyclic cascade assembly, a multifunctional guest molecule, namely alkyl-bridged triphenylamine-vinyl pyridine salts BTPA, was synthesized, in which the flexible chains and pyridine cation made it possible to form a foldamer binding with CB[8], and the methoxy phenyl group enabled complexation with β-cyclodextrin (β-CD) for secondary assembly. The synthesis route and characterization data, including ^{1}H NMR, ^{13}C NMR, HR-MS of BTPA, PY, and reference molecules (BPA and TPA), are summarized in the supporting information (Figures S1–S4, Supporting Information).

For the first-order self-assembly BTPA/CB[8], the experiments of ^{1}H NMR and 2D correlation spectroscopy (COSY) (Figure S6, Supporting Information) have been performed to explore the host-guest binding behaviors. As shown in **Figure** 1a and Figure S5 (Supporting Information), the protons in styryl pyridiniums groups experienced a shift toward the high field (H_1, H_2, H_3, H_4, and H_5) upon gradual addition of CB[8], indicating a deep encapsulation of the styryl pyridiniums groups within the CB[8] cavity. In contrast, the proton in the methoxyphenyl group exhibited a downfield shift (H_6/H_6' and Ha), implying that these protons existed outside the cavity. Furthermore, the UV spectrums titration experiment demonstrated, with the stepwise addition of CB[8] to the guest solution, the absorption of guest BTPA was redshifted from 480 to 520 nm, and the corresponding association constant (K_s) of BTAP/CB[8] was obtained to be 4.07×10^6 M^{-1} (Figure 1b; Figure S7, Supporting Information). Job's plot confirmed a 1:1 stoichiometry for BTPA/CB[8] (Figure S8, Supporting Information), which was also supported by HR-MS analysis, wherein the molecular ion peak of BTPA/CB[8] (m/z: 1093.89418) corresponded to the calculated value of 1:1 complex with an m/z of 1093.90468 (Figure S9, Supporting Information). Additionally, 2D rotating frame overhauser effect spectroscopy (ROESY) and 2D diffusion-ordered spectroscopy

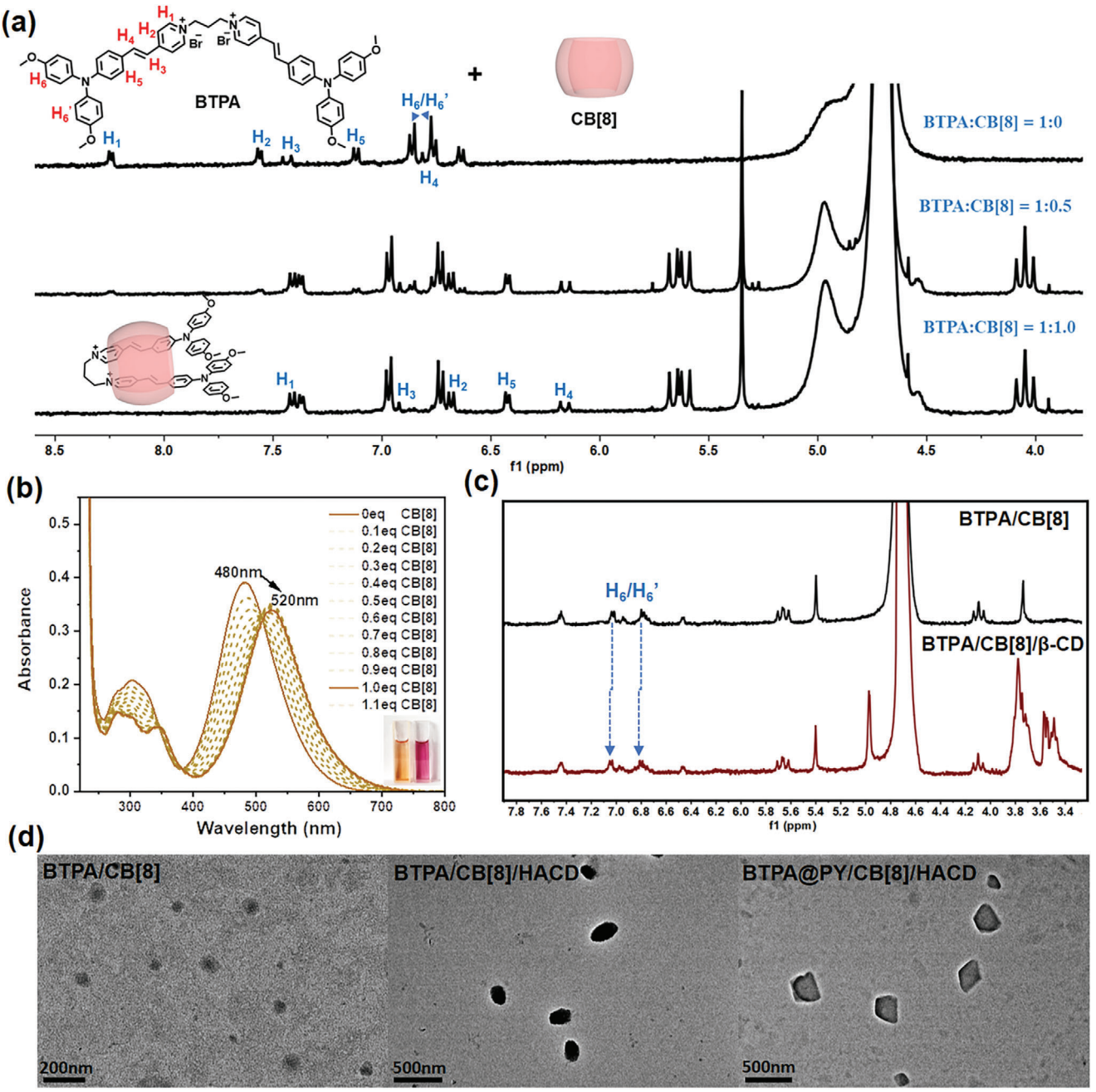

Figure 1. a) ^{1}H NMR spectral changes of BTPA after adding 0, 0.5, and 1.0 equivalent CB[8]. (400 MHz, D_2O with 5%CD_3OD, 298 K); b) UV–vis absorption spectra of aqueous solutions of BTPA (10 μM) and CB[8] (0 to 1.1 equivalent) under ambient conditions. Inset: the picture of BTPA (left) and BTPA/CB[8] (right). c) ^{1}H NMR spectra of BTPA/CB[8] and BTPA/CB[8]/β-CD ([BTPA] = [CB[8]] = 0.1 mM; [β-CD] = 0.2 mM). (400 MHz, D_2O with 5%DMSO-*d6*, 298 K) d) TEM image of BTPA/CB[8] ([BTPA] = [CB[8]] = 10 μM), BTPA/CB[8]/HACD ([BTPA] = [CB[8]] = 10 μM; [HACD] = 0.02 mg ml^{-1}) and BTPA@PY/CB[8]/HACD ([BTPA] = 10 μM; [PY] = 0.1 mM; [CB[8]] = 60 μM; [HACD] = 0.02 mg ml^{-1}).

(DOSY) were implemented to gain further insight into the assembly details. The correlation peaks between protons on pyridine (H_1) and protons on the double bond (H_3, H_4) corroborated the folding mode for BTPA (Figure S10, Supporting Information). The diffusion coefficients of BTPA (3.33×10^{-10} m^2 s^{-1}) and BTPA/CB[8] (2.54×10^{-10} m^2 s^{-1}) remained relatively stable, excluding the possibility of the formation of chain supramolecular polymers (Figure S11, Supporting Information). Integrated with the above results, the formation of a 1:1 complex between BTPA and CB[8] in a "head-to-head" folding mode was confirmed.

Benefiting from the stronger host-guest complexation between hydrophobic cavities of β-CD and aromatic guest molecules, as well as the electronegativity of HA, HACD was further introduced into BTPA/CB[8] system in anticipation of facilitating the cascade assembly through multivalent interaction. In detail, the ^{1}H NMR spectra showed that upon the addition of

β-CD, the protons on methoxyphenyl (H_6 and H_6') in BTPA/CB[8] shifted slightly to low-field, while the proton in styryl pyridiniums remained unchanged (Figure 1c), indicating the complexation of β-CD and methoxyphenyl unit. For the reference molecule (TPA) without alkyl-bridged, similar downfield shifts were observed for the methoxyphenyl protons, which was in accord with BTPA/CB[8] (Figure S12, Supporting Information), and the association constant of TPA/β-CD has obtained $K_s = 4.33 \times 10^3$ M^{-1} (Figure S13, Supporting Information). These experimental results consistently indicated that the methoxyphenyl units provide a binding site to be accommodated by β-CD, facilitating the non-covalent polymerization between BTPA/CB[8] and HACD. And then, the stoichiometric 2:1 PY and CB[8] complex[13] were doped in BTPA/CB[8]/HACD system to form a more compact supramolecular assembly. Control experiments demonstrated, upon the gradual addition of CB[8], the phenyl protons on PY were shifted to the high field, and the passivation chemical shifts occurred on the alkyl chains with almost no change in shift, and it was found that the proton chemical shift changes of PY came to an equilibrium state with 0.5 equivalent CB[8] (Figure S14, Supporting Information). Furthermore, after the continuous addition of β-CD in the current system, the protons on alkyl chains de-passivated and shifted downfield slightly (Figure S15, Supporting Information). These results showed that β-CD could bind not only with the aromatic rings in BTPA but also with the alkyl chains in PY/CB[8], confirming that the formation of cascade supramolecular assembly was driven by multivalent interactions.

The multivalent assembly progress of BTPA/CB[8] with HACD and PY/CB[8] was further validated through various characterization techniques, including transmission electron microscopy (TEM), scanning electron microscopy (SEM), dynamic light scattering (DLS), Tyndall experiments, and zeta potential experiments. TEM, SEM, and DLS results showed that the assembly BTPA/CB[8] formed spherical nanoparticles with a diameter of ≈100 nm, which transformed into ellipsoidal nanoparticles with a diameter of ≈250 nm upon secondary assembly with HACD. Subsequently, polyhedral particles with a doubled particle size of ≈450 nm were obtained through co-assembly with PY/CB[8] (Figure 1d; Figure S16, Supporting Information). Tyndall experiments also evidenced such results, in which BTPA and BTPA/CB[8] exhibited a fragile Tyndall effect, while BTPA/CB[8]/HACD and BTPA@PY/CB[8]/HACD revealed a strong Tyndall effect (Figure S17, Supporting Information). The average zeta potential of BTPA/CB[8] was +7.73 mV, BTPA/CB[8]/HACD and BTPA@PY/CB[8]/HACD had an average zeta potential of −11.96 and −6.90 mV, respectively (Figure S18, Supporting Information). Based on these experimental results, a stable cascade self-assembly nanoparticle was successfully constructed through multivalent interactions based on host-guest binding.

It was significant that the supramolecular cascade assembly exhibited continued enhanced fluorescence and phosphorescence behavior. The UV–vis spectrum showed a redshift of the maximum absorption peak of BTPA from 480 to 520 nm after binding with CB[8], which further blueshifted to 500 nm with co-assembly by HACD (**Figure 2**a). BTPA@PY/CB[8]/HACD showed a peak at ≈305 and 500 nm, which were assigned to the PY/CB[8] unit[14] and BTPA/CB[8] section, respectively. The steady-state photoluminescence spectra indicated a phenomenon of cascade-enhanced NIR luminescence resulting from multivalent self-assembly (Figure 2b). Concretely, in the first-order self-assembly, the addition of CB[8] caused the maximum emission peak to redshift from 720 to 750 nm (λ_{ex} = 520 nm) along with a 14-fold increase in quantum yield from 0.06% to 0.88% (Figure 2b,c). This enhancement reached an equilibrium state at 0.5 equivalent CB[8], confirming the 1:1 single molecular folds-dimer assembly between BTPA and CB[8]. In the secondary self-assembly with HACD, the emission of BTPA/CB[8]/HACD further redshifted to 810 nm (λ_{ex} = 500 nm), and the quantum yield concurrently increased eightfold to 7.21% due to the multivalent interaction between BTPA/CB[8] and HACD (Figure 2b,c). After introducing the PY/CB[8], a more compact supramolecular assembly was formed, and the quantum yield of BTPA@PY/CB[8]/HACD increased by 3-fold to 22.92% compared to BTPA/CB[8]/HACD. While the maximum emission peak experienced a certain blueshift to 780 nm (λ_{ex} = 500 nm), which may be attributed to the decreased polarity of the chromophore environment caused by the dense aggregation (Figure 2b,c). Moreover, the fluorescence lifetime was extended from 0.67 to 1.78 ns through this three-stage assembly, corroborating the emergence of a multivalent self-assembly process (Figure S19, Supporting Information). It has been proved that 4-bromophenylpyridine derivatives can produce the desired CB[8]-induced RTP in aqueous solution.[14–15] Regarding the phosphorescence properties, it was found that PY exhibited phosphorescence emission at 510 nm (λ_{ex} = 305 nm) after adding CB[8], and the phosphorescence intensity was significantly enhanced upon the gradual addition of HACD with a final lifetime recording to 230.27 μs (Figure 2d; Figure S20, Supporting Information). This improvement was ascribed to the restriction effect of CB[8] and β-CD on PY and the shielding effect of aggregates against quenchers such as oxygen and water. As expected, BTPA@PY/CB[8]/HACD also exhibited intense phosphorescence at 510 nm with a lifetime of 140.2 μs (Figure 2d). The luminescence intensity and lifetime in the nitrogen atmosphere were greatly enhanced than the one under aerated conditions, confirming the phosphorescent properties (Figure S21, Supporting Information). These results indicated that supramolecular multivalent self-assembly was an effective strategy for achieving cascade-enhanced luminescence and double emission of fluorescence-phosphorescence.

To investigate the influence of methoxyphenyl and the aliphatic chain of guest molecules on cascade assembly-induced optical changes, BPA without methoxyphenyl group and PY-1 with no alkyl chain were synthesized. Compared with BTPA's multivalent assembly that exhibited a greatly cascade-enhanced luminescent effect, the fluorescence of BPA was quenched with the addition of CB[8] (Figure S22, Supporting Information) and exhibited a weaker luminescent enhancement effect with emission intensity increased by 1.5 times upon the further addition of HACD (Figure S23, Supporting Information). Binary assembly BPA/HACD showed a similar phenomenon, in which the fluorescence intensity of BPA improved by only 1.6 times for secondary self-assembly with HACD, whereas BTPA exhibited a 12-fold enhancement. (Figure S24, Supporting Information). These results directly confirmed the cascade-enhanced luminescent process resulting from the host-guest interactions between methoxyphenyl units and β-CD. Furthermore, the emission

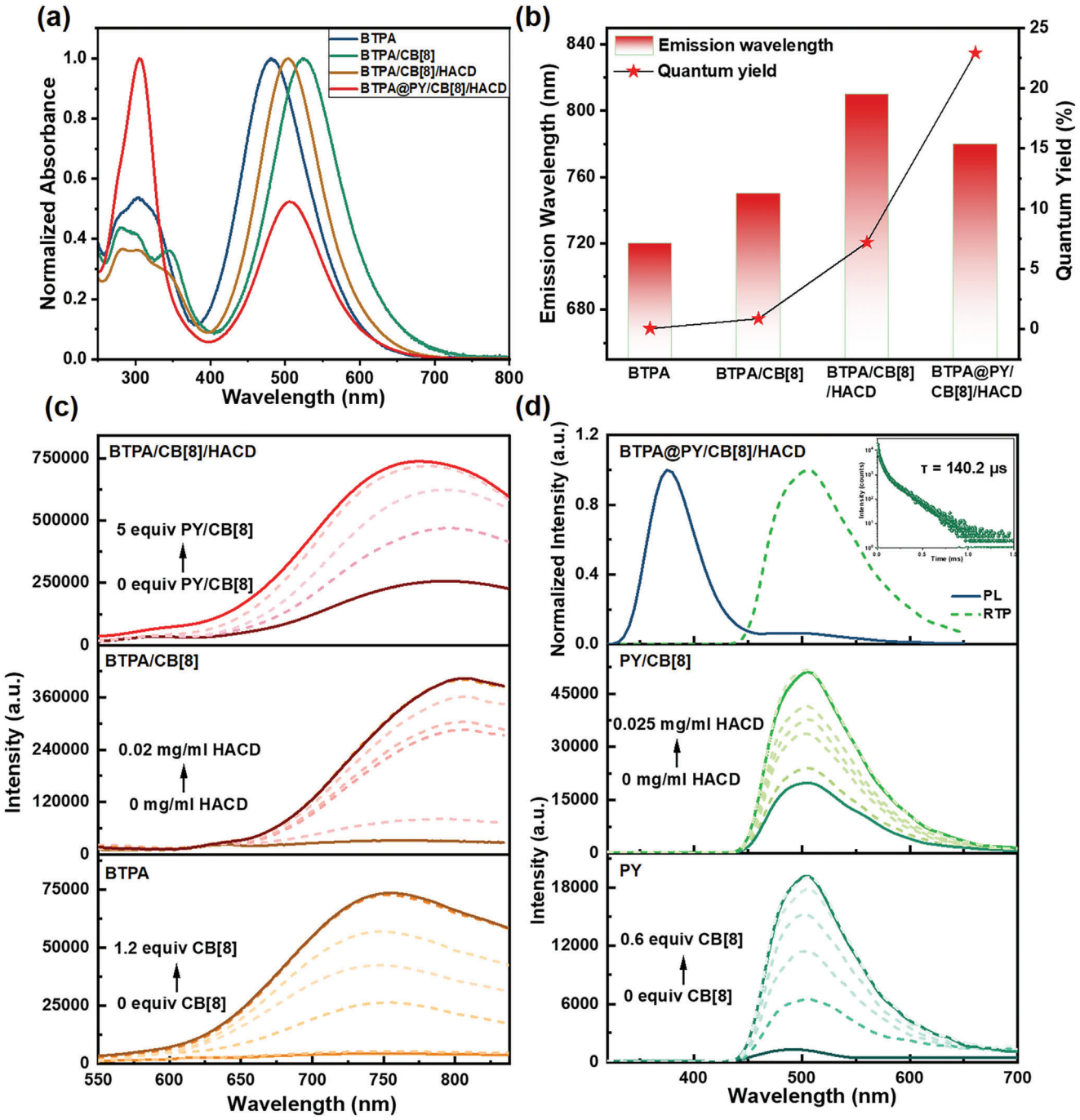

Figure 2. a) UV–vis absorption spectra of BTPA, BTPA/CB[8], BTPA/CB[8]/HACD, and BTPA@PY/CB[8]/HACD. b) The maximum emission wavelength and quantum yield of BTPA, BTPA/CB[8], BTPA/CB[8]/HACD and BTPA@PY/CB[8]/HACD. c) PL spectra of BTPA upon the addition of 0, 0.2, 0.4, 0.6, 0.8, 1.0, 1.2 equiv CB[8] in aqueous solution (Bottom) ([BTPA] = 10 μM; λ_{ex} = 520 nm); PL spectra of BTPA/CB[8] upon the addition of 0, 0.002, 0.004, 0.008, 0.012, 0.016, 0.02 mg ml^{-1} HACD in aqueous solution (Middle) ([BTPA] = [CB[8]] = 10 μM; λ_{ex} = 500 nm); PL spectra of BTPA/CB[8]/HACD upon the addition of 0, 2.0, 3.0, 4.0, 5.0 equiv PY/CB[8] in aqueous solution (Top) ([BTPA] = [CB[8]] = 2 μM; [HACD] = 0.004 mg ml^{-1}; λ_{ex} = 500 nm); d) Bottom: Phosphorescence spectra of PY upon the addition of 0, 0.1, 0.2, 0.3, 0.4, 0.5, 0.6 equiv CB[8] ([PY] = 10 μM); Middle: Phosphorescence spectra of PY/CB[8] upon the addition of 0, 0.0025, 0.005, 0.01, 0.015, 0.02, 0.025 mg ml^{-1} HACD ([PY] = 2[CB[8]] = 10 μM); TOP: PL spectra and phosphorescence spectra of BTPA@PY/CB[8]/HACD ([BTPA] = 2 μM; [PY] = 10 μM; [CB[8]] = 7 μM; [HACD] = 0.004 mg ml^{-1}; λ_{ex} = 305 nm). Inset: time-resolved PL decay curves of BTPA@PY/CB[8]/HACD record at 510 nm. All phosphorescence spectra were recorded with a delay time of 100 μs.

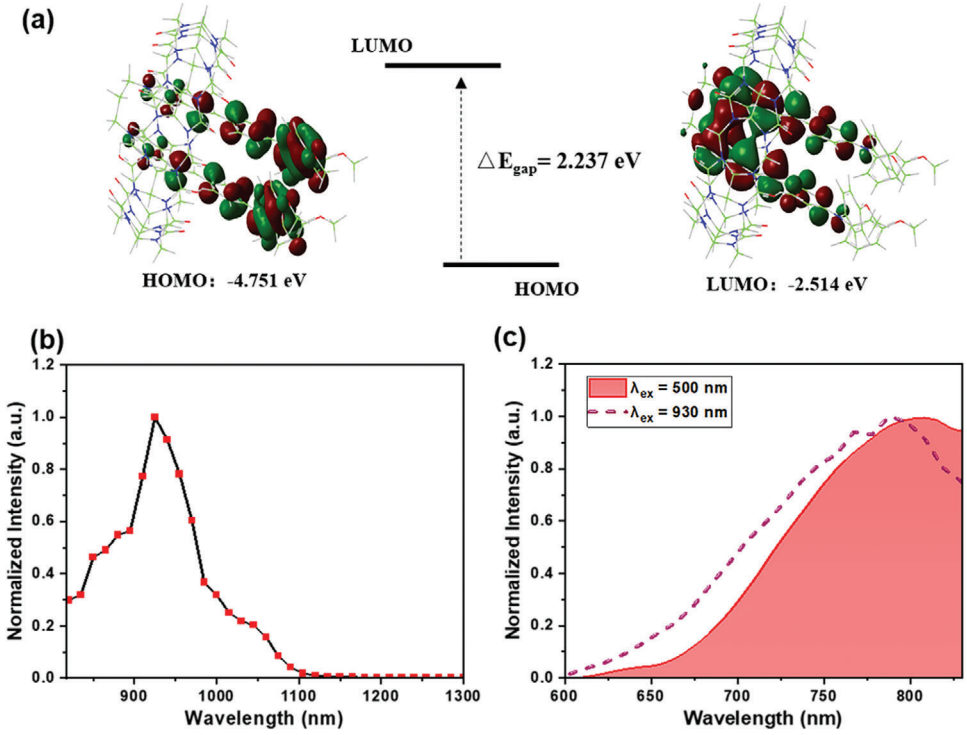

Figure 3. a) The calculated spatial distributions of HOMO and LUMO for BTPA/CB[8]. b) Two-photon excitation spectrum of BTPA/CB[8]/HACD in aqueous solution under ambition conditions. c) Two-photon and single-photon emission spectra of assembly BTPA/CB[8]/HACD excited with different wavelengths in aqueous. ([BTPA] = [CB[8]] = 10 μM; [HACD] = 0.02 mg ml^{-1}).

intensity of BTPA/CB[8]/HACD hardly changed with the addition of 7.5 equivalent PY-1/CB[8] (Figure S25, Supporting Information), indicating that alkyl chains binded with β-CD were crucial to the cascaded enhanced luminescence effect. Therefore, the excellent luminescence performance of BTPA@PY/CB[8]/HACD was primarily ascribed to the noncovalent polymerization effect based on the stepwise encapsulation of methoxyphenyl partial and hydrophobic dodecyl chain by β-CD on the HA surface, thereby leading to the formation of multivalent interactions, including hydrophobic interaction, electrostatic attraction interactions, and host-guest interactions, ultimately achieving cascade luminescent enhancement effect with double emission of phosphorescence and fluorescence.

Notably, the typical D-π-A structure of BTPA structure may cause a strong charge transfer effect that favors the two-photon absorption. Density functional theory (DFT) calculation showed that the HOMO orbital of BTPA/CB[8] was mainly located on the two methoxyphenyl groups. At the same time, the LUMO was mainly localized over the pyridine groups (**Figure 3**a). The small degree of absolute orbital overlap hinted at the possible ICT process, in which electrons could be transferred from methoxyphenyl to pyridine units when BTPA/CB[8] was excited. Thus, we further investigated the two-photon absorption properties of these supramolecular assemblies with strong NIR emission properties. As expected, BTPA/CB[8]/HACD's excitation wavelength ranges were recorded at 850–1100 nm (Figure 3b). The fluorescence spectra of BTPA/CB[8]/HACD at a two-photon 930 nm excited femtosecond laser showed a similar emission peak with the spectra under 500 nm one-photon excitation (Figure 3c). Likewise, tertiary supramolecular assembly BTPA@PY/CB[8]/HACD also showed significant two-photon absorption, which emitted NIR fluorescence under a 930 nm excited femtosecond laser irradiation (Figure S26, Supporting Information).

In light of the two-photon absorption properties of BTPA@PY/CB[8]/HACD and the targeted cancer cells' ability of HA, we further explored the fluorescence and phosphorescence targeted imaging behavior. Two kinds of cancer cells, including human cervical carcinoma cells (HeLa cells) and human lung adenocarcinoma cells (A549 cells), and a normal human embryonic kidney cell (293T cells), were respectively incubated with BTPA@PY/CB[8]/HACD (2 μM) for 12 h. Two-photon confocal laser scanning microscopy (CLSM) was used for cell imaging. The results showed that a green phosphorescence belonging to PY/CB[8] was observed under excitation by a 405 nm laser, and the NIR luminescence in the cytoplasm was excited by a 488 nm laser as well as a 930 nm femtosecond pulsed laser for HeLa cells (**Figure 4**a). Moreover, both of these two cancer cells exhibited bright green and red signals, whereas almost no emission signal was observed in 293T cells, implying that BTPA@PY/CB[8]/HACD was more preferentially internalized by cancer cells than normal cells benefiting from the HA receptor-mediated endocytosis (Figure 4; Figure S27, Supporting Information). The merged imaging with a Pearson's coefficient of 0.84 in HeLa cells and 0.79 in A549 cells verified the colocalization of NIR fluorescence and green phosphorescence, indicating the stability of the assembly in cells (Figure S28, Supporting Information). CCK-8 assays were

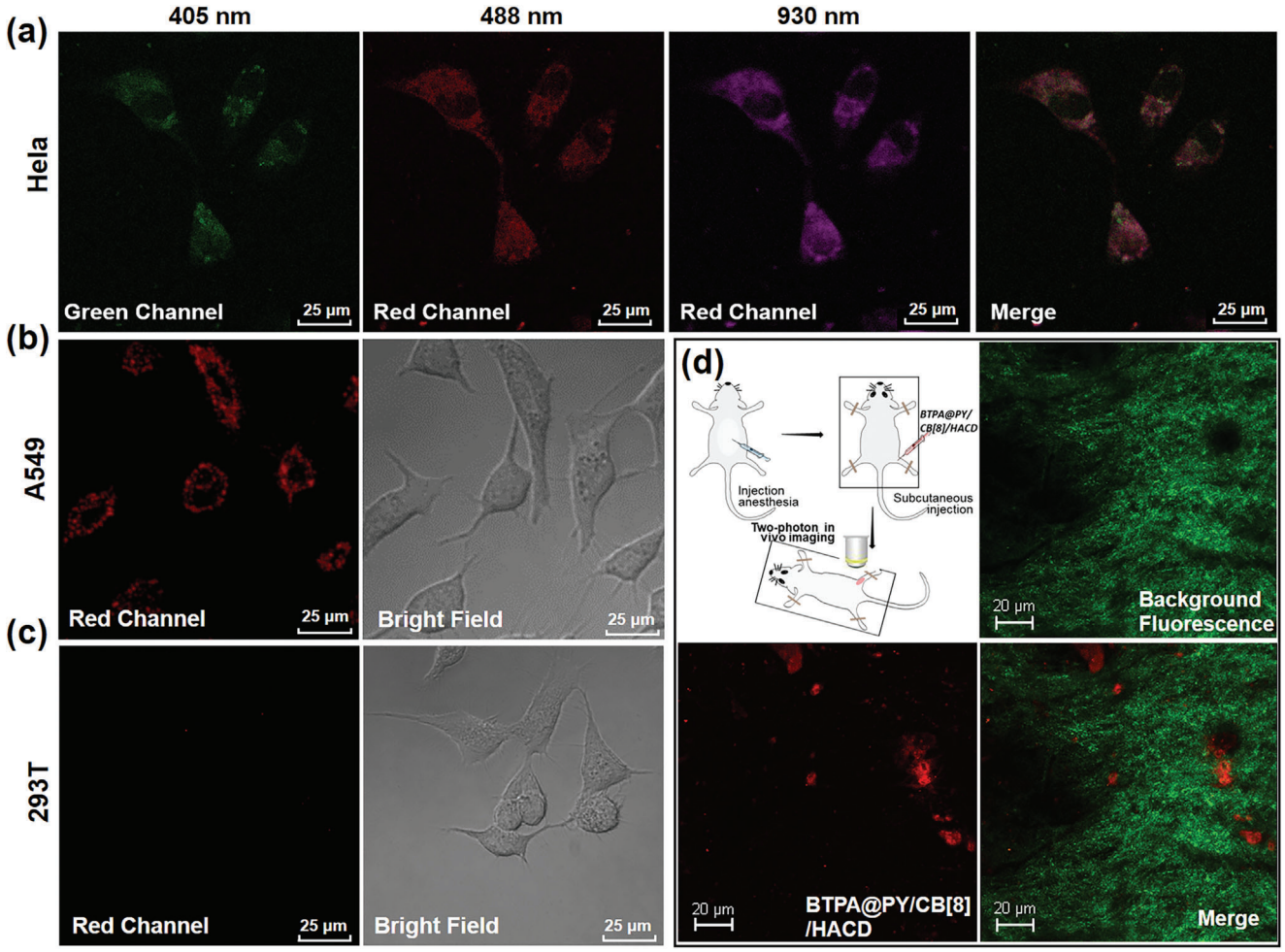

Figure 4. a) Cell imaging of Hela cancer cells incubated with BTPA@PY/CB[8]/HACD excited by 405 nm excitation light, 488 nm excitation light, 930 nm femtosecond pulsed laser, and merged imaging. (Green channel: 450 – 550 nm, red channel: 650 – 800 nm). b,c) Cell imaging of A549 cancer cells and 293T normal cells incubated with BTPA@PY/CB[8]/HACD excited by 405 nm excitation light. (Red channel: 650 – 800 nm). d) Vivo mouse subcutaneous tissue imaging of autofluorescence from background interference, BTPA@PY/CB[8]/HACD, and merged imaging. (Excitation: 930 nm; green channel: 450 – 530 nm, red channel: 650 – 800 nm).

conducted to evaluate cytotoxicity experiments on the above three cells, and the high survival rate indicated low cytotoxicity of the assembly BTPA@PY/CB[8]/HACD (Figure S29, Supporting Information). Compared with single-photon imaging, the two-photon imaging stimulated by the NIR femtosecond pulse laser offers higher penetration and signal-to-noise ratio, materializing a unique advantage for in vivo imaging. Subsequently, BTPA@PY/CB[8]/HACD (2 μM) was injected into the hind leg of live mice to carry out subcutaneous tissue imaging experiments. Under 930 nm femtosecond pulsed laser excitation, the NIR luminescent signal (red) was clearly observed by confocal microscopy, effectively eliminating the background autofluorescence (green) interference caused by bio-tissue proteins (Figure 4d, Supporting Information).

3. Conclusion

In summary, a conformation confined multivalent supramolecular cascade-enhanced luminescence system with green phosphorescence and two-photon NIR fluorescence was fabricated by the co-assembly of BTPA, PY, CB[8], and HACD, which exhibited continuous redshift emission from 720 to 780 nm and significant increase in quantum yield from 0.06% to 22.92%. The first-order macrocyclic confinement of CB[8] driven BTPA folding, resulting in the primary enhanced luminescence effect. The subsequent secondary assembly with HACD further extended the NIR emission region and increased the quantum yield by 120-fold through multivalent interactions. The further co-assembly with PY/CB[8] promoted the formation of dense supramolecular nanoparticles, finally achieving stronger NIR fluorescence with continuously increasing quantum yield by 3-fold as well as endowing green phosphorescent emission. Cellular and in vivo imaging experiments illustrated that the macrocyclic supramolecular cascade assembly was successfully utilized for targeted imaging of cancer cells, which effectively shielded the interference of background spontaneous fluorescence and phosphorescence, revealing its great potential application in biological theragnostic.

Supporting Information

Supporting Information is available from the Wiley Online Library or from the author.

Acknowledgements

This work was financially supported by the National Natural Science Foundation of China (NNSFC, Grant Nos. 22131008).

Conflict of Interest

The authors declare no conflict of interest.

Data Availability Statement

The data that support the findings of this study are available from the corresponding author upon reasonable request.

Keywords

cascade enhanced luminescence, phosphorescence, supramolecular assembly, two-photon NIR fluorescence

Received: June 30, 2023
Revised: August 4, 2023
Published online:

[1] a) J. Yang, Y. Zhang, X. Wu, W. Dai, D. Chen, J. Shi, B. Tong, Q. Peng, H. Xie, Z. Cai, Y. Dong, X. Zhang, *Nat. Commun.* **2021**, *12*, 4883; b) X. Li, W. Tan, X. Bai, F. Li, *Chem. Res. Chin. Univ.* **2023**, *39*, 192; c) H. Lu, Y. Zheng, X. Zhao, L. Wang, S. Ma, X. Han, B. Xu, W. Tian, H. Gao, *Angew. Chem., Int. Ed.* **2016**, *55*, 155; d) W. Zou, Y. Zhu, C. Gu, Y. Miao, S. Wang, B. Yu, Y. Shen, H. Cong, *J. Mater. Sci.* **2020**, *55*, 9918.

[2] a) S. Lu, L. Sui, J. Liu, S. Zhu, A. Chen, M. Jin, B. Yang, *Adv. Mater.* **2017**, *29*, 1603443; b) F.-F. Shen, Y. Chen, X. Xu, H.-J. Yu, H. Wang, Y. Liu, *Small* **2021**, *17*, 2101185; c) Y. Wang, H. Wu, P. Li, S. Chen, L. O. Jones, M. A. Mosquera, L. Zhang, K. Cai, H. Chen, X.-Y. Chen, C. L. Stern, M. R. Wasielewski, M. A. Ratner, G. C. Schatz, J. F. Stoddart, *Nat. Commun.* **2020**, *11*, 4633; d) X.-K. Ma, X. Zhou, J. Wu, F.-F. Shen, Y. Liu, *Adv. Sci.* **2022**, *9*, 2201182.

[3] a) G. Qian, Z. Zhong, M. Luo, D. Yu, Z. Zhang, D. Ma, Z. Y. Wang, *J. Phys. Chem. C* **2009**, *113*, 1589; b) Z. Wang, L. Yan, L. Zhang, Y. Chen, H. Li, J. Zhang, Y. Zhang, X. Li, B. Xu, X. Fu, Z. Sun, W. Tian, *Polym. Chem.* **2014**, *5*, 7013; c) G. Lijuan, W. Kaizhen, W. Yuxin, Y. Jun, L. Xian, G. Jingxuan, L. Ji, D. Dawei, C. Haiyan, Y. Zhenwei, *Chin. Chem. Lett.* **2023**, *34*, 107586.

[4] a) W. Qin, D. Ding, J. Liu, W. Z. Yuan, Y. Hu, B. Liu, B. Z. Tang, *Adv. Funct. Mater.* **2012**, *22*, 771; b) Y.-J. Yu, Y. Hu, S.-Y. Yang, W. Luo, Y. Yuan, C.-C. Peng, J.-F. Liu, A. Khan, Z.-Q. Jiang, L.-S. Liao, *Angew. Chem., Int. Ed.* **2020**, *59*, 21578; c) I. Javed, T. Zhou, F. Muhammad, J. Guo, H. Zhang, Y. Wang, *Langmuir* **2012**, *28*, 1439; d) Y. Fan, F. Wang, F. Hou, L. Wei, G. Zhu, D. Zhao, Q. Hu, T. Lei, L. Yang, P. Wang, G. Ge, *Chin. Chem. Lett.* **2023**, *34*, 107557.

[5] a) Y. Rong, R. Liu, P. Jin, C. Liu, X. Wang, L. Fang, L. Chen, W. Wu, C. Yang, *J. Mater. Chem. A* **2023**, *11*, 5895; b) X. Yu, S. Wan, W. Wu, C. Yang, W. Lu, *Chem. Commun.* **2022**, *58*, 6284; c) X. Chen, H. K. Bisoyi, X.-F. Chen, X.-M. Chen, S. Zhang, Y. Tang, G. Zhu, H. Yang, Q. Li, *Matter* **2022**, *5*, 3883; d) X.-M. Chen, X. Chen, X.-F. Hou, S. Zhang, D. Chen, Q. Li, *Nanoscale Adv.* **2023**, *5*, 1830.

[6] a) X. Song, F. Liu, S. Sun, J. Wang, J. Cui, X. Peng, *RSC Adv.* **2014**, *4*, 9326; b) J.-L. Zhou, Y.-H. Li, Y.-M. Zhang, L. Chen, Y. Liu, *Org. Biomol. Chem.* **2023**, *21*, 107; c) Y. Tang, H. K. Bisoyi, X.-M. Chen, Z. Liu, X. Chen, S. Zhang, Q. Li, *Adv. Mater.* **2023**, *35*, 2300232; d) N. Qian, X.-F. Hou, Y. Tang, S. Zhang, X.-M. Chen, Q. Li, *ChemPhotoChem* **2023**, *7*, 202300018; e) X.-F. Hou, X.-M. Chen, H. K. Bisoyi, Q. Qi, T. Xu, D. Chen, Q. Li, *ACS Appl. Mater. Interfaces* **2023**, *15*, 11004; f) X.-F. Hou, S. Zhang, X. Chen, H. K. Bisoyi, T. Xu, J. Liu, D. Chen, X.-M. Chen, Q. Li, *ACS Appl. Mater. Interfaces* **2022**, *14*, 22443.

[7] S. Garain, B. C. Garain, M. Eswaramoorthy, S. K. Pati, S. J. George, *Angew. Chem., Int. Ed.* **2021**, *60*, 19720.

[8] J. Wang, Z. Huang, X. Ma, H. Tian, *Angew. Chem., Int. Ed.* **2020**, *59*, 9928.

[9] B. Shi, K. Jie, Y. Zhou, J. Zhou, D. Xia, F. Huang, *J. Am. Chem. Soc.* **2016**, *138*, 80.

[10] X.-M. Chen, Y. Chen, Q. Yu, B.-H. Gu, Y. Liu, *Angew. Chem., Int. Ed.* **2018**, *57*, 12519.

[11] a) W.-W. Xing, H.-J. Wang, Z. Liu, Z.-H. Yu, H.-Y. Zhang, Y. Liu, *Adv. Opt. Mater.* **2023**, *11*, 2202588; b) M. Huo, X.-Y. Dai, Y. Liu, *Adv. Sci.* **2022**, *9*, 2201523; c) M. Huo, X.-Y. Dai, Y. Liu, *Angew. Chem., Int. Ed.* **2021**, *60*, 27171; d) J.-J. Li, Y. Chen, J. Yu, N. Cheng, Y. Liu, *Adv. Mater.* **2017**, *29*, 1701905; e) G. Sun, W. Qian, J. Jiao, T. Han, Y. Shi, X.-Y. Hu, L. Wang, *J. Mater. Chem. A* **2020**, *8*, 9590.

[12] a) X. Tian, M. Zuo, P. Niu, K. Wang, X. Hu, *Chin. J. Org. Chem.* **2020**, *40*, 1823; b) X.-L. Ni, X. Xiao, H. Cong, Q.-J. Zhu, S.-F. Xue, Z. Tao, *Acc. Chem. Res.* **2014**, *47*, 1386; c) H. Yang, B. Yuan, X. Zhang, O. A. Scherman, *Acc. Chem Res.* **2014**, *47*, 2106; d) L. Yue, K. Yang, X.-Y. Lou, Y.-W. Yang, R. Wang, *Matter* **2020**, *3*, 1557; e) X.-K. Ma, Y. Liu, *Acc. Chem. Res.* **2021**, *54*, 3403; f) S.-H. Li, X. Xu, Y. Zhou, Q. Zhao, Y. Liu, *Org. Lett.* **2017**, *19*, 6650.

[13] X.-Y. Dai, M. Huo, X. Dong, Y.-Y. Hu, Y. Liu, *Adv. Mater.* **2022**, *34*, 2203534.

[14] F.-F. Shen, Z. Liu, H.-J. Yu, H. Wang, X. Xu, Y. Liu, *Adv. Opt. Mater.* **2022**, *10*, 2200245.

[15] X.-K. Ma, Y.-M. Zhang, Q. Yu, H. Zhang, Z. Zhang, Y. Liu, *Chem. Commun.* **2021**, *57*, 1214.